Evaluation of Sea Surface Temperatures Derived From the HY-1D Satellite

Xiaomin Ye, Jianqiang Liu, Mingsen Lin, *Member, IEEE*, Jing Ding, Bin Zou, Qingjun Song, and Yue Teng

***Abstract*—Global sea surface temperatures (SSTs) are detected by the Chinese ocean color and temperature scanner (COCTS) instruments aboard the HaiYang (HY)-1C and HY-1D satellites. In this study, the SSTs derived from the COCTS instrument on the HY-1D (COCTS/HY-1D) satellite and a nonlinear SST algorithm with corresponding coefficients were introduced. The COCTS/HY-1D SSTs recorded from April 26 to August 31, 2021, were evaluated against water temperature measurements taken at depths above 1 m from the *in situ* Quality Monitor system; root-mean-square errors (RMSEs) of 0.65 and 0.71 °C and robust standard deviations (RSDs) of 0.51 and 0.47 °C were obtained for the daytime and nighttime SSTs, respectively, using a spatiotemporal matching window of 4 h and 2.5 km. Daily gridded SSTs derived from COCTS/HY-1D were compared with those obtained from the visible infrared imaging radiometer suite (VIIRS) aboard the Suomi National Polar-orbiting Partnership (S-NPP) satellite in the same period, and RMSEs of 0.67 ± 0.06 and 0.81 ± 0.06 °C and RSDs of 0.49 ± 0.04 and 0.58 ± 0.05 °C were obtained for the daytime and nighttime SSTs, respectively. The COCTS/HY-1D-derived SSTs covering Gulf Stream waters were cross-validated against the VIIRS/S-NPP data as a case study, and RMSEs of 0.53 and 0.47 °C for the daytime and nighttime, respectively, were obtained.**

***Index Terms*—Chinese ocean color and temperature scanner (COCTS), HaiYang (HY)-1D satellite, sea surface temperature (SST), validation.**

I. Introduction

SEA surface temperature (SST), defined as the skin temperature of the ocean surface water, is a key measurement for ocean, weather, and climate research and can be applied in numerical oceanic and atmospheric models, fishery science, and for the tactical support of commercial fishing activities, physical oceanographic research, and climate monitoring [1]–[7]. SSTs derived from spaceborne sensors can be obtained from both the microwave and infrared (IR) bands, and satellites can cover global oceans or local seas multiple times in each day [8]. IR radiometers, such as the advanced very high resolution radiometer, moderate-resolution imaging spectroradiometer (MODIS), sea and land surface temperature radiometer, visible infrared imaging radiometer suite (VIIRS), and Chinese ocean color and temperature scanner (COCTS), have been providing global SSTs for more than 40 years at spatial scales of ∼1 km [9]–[11].

In general, IR radiometers measure SSTs using the brightness temperatures (BTs) of thermal infrared (TIR) bands at 11 and 12 μm or using TIR bands combined with the mid-IR band (e.g., at 3.7 μm for VIIRS) by applying split-window algorithms (e.g., the multichannel SST (MCSST) algorithm [10] and the nonlinear SST (NLSST) algorithm [1]), physical models based on radiative transfer model simulations [12], [13], or neural network models [14]). SST retrieval algorithms can be developed for the global ocean [15]–[17] or for regional marine waters [18]–[20]. Correspondingly, satellite-derived remote sensing SSTs have been evaluated and validated in both global ocean and regional waters [18], [21]–[28]. For example, Lee *et al.* [23], Petrenko *et al.* [15], Hao *et al.* [26], and Gentemann [22] evaluated MODIS-derived SSTs in the waters around Taiwan, in the South China Sea, in the coastal waters of the Yellow Sea, and in the global ocean, respectively. Evaluation results may not be consistent among different marine areas. For example, the root-mean-square errors (RMSEs) of the SSTs derived from the MODIS sensors on the Terra and Aqua satellites were found to be 0.83 and 0.71 °C, respectively, in the waters around Taiwan [23]. These corresponding RMSEs were 0.83 and 0.85 °C, respectively, with standard deviations (SDs) of 0.79 and 0.85 °C, respectively, in the coastal waters of the Yellow Sea [26], while the SD of the SSTs derived from the MODIS instrument aboard Aqua was found to be 0.56 °C for the global ocean [22].

New remote sensing products or retrieval algorithms should be evaluated to determine their accuracies in specific water areas. For example, Wang *et al.* [27] evaluated SSTs derived from Fengyun-3C visible and infrared radiometer data collected in the Arctic. Koner [21] validated daytime SSTs using a retrieval algorithm incorporating midwave imager measurements. Ye *et al.* [11] evaluated the SSTs derived from the COCTS on the HaiYang (HY)-1C satellite.

HY-1D, a new satellite designed by China for the global ocean color and SST detections, was launched in June 2020. The COCTS, which can monitor the global ocean color and the sea surface temperature every day, is the key payload aboard the HY-1D satellite. As a spaceborne sensor designed for global ocean color and SST monitoring, the performance of the SST products output by the COCTS should be evaluated. In this study,

Manuscript received October 1, 2021; revised November 28, 2021; accepted December 14, 2021. Date of publication December 21, 2021; date of current version January 6, 2022. This work was supported by the National Natural Science Foundation of China under Grant 41876211, Grant 41876204, and Grant 41506206. *(Corresponding author: Xiaomin Ye.)*

Xiaomin Ye, Jianqiang Liu, Mingsen Lin, Jing Ding, Bin Zou, Qingjun Song, and Yue Teng are with the National Satellite Ocean Application Service, Beijing 100081, China, and also with the Key Laboratory of Space Ocean Remote Sensing and Application, Ministry of Natural Resources, Beijing 100081, China (e-mail: yexiaomin2011@foxmail.com; jqliu@mail.nsoas.org.cn; mslin@mail.nsoas.org.cn; dingjing@mail.nsoas.org.cn; zoubin@mail.nsoas.org.cn; kingdream@mail.nsoas.org.cn; 1136459681@qq.com).

Digital Object Identifier 10.1109/JSTARS.2021.3137230

the SSTs derived from the COCTS on HY-1D (COCTS/HY-1D) were evaluated through comparisons with both *in situ* data and the SST products derived from the VIIRS on the Suomi National Polar-orbiting Partnership (VIIRS/S-NPP).

The rest of this article is organized as follows. Section II introduces the SST data products of COCTS/HY-1D and VIIRS/S-NPP, water temperature measurements from the National Oceanic and Atmospheric Administration (NOAA) *in situ* Quality Monitor (iQuam) system, and the data match-up and evaluation methodology. Section III presents the evaluation results obtained by comparing the COCTS/HY-1D data to both *in situ* measurements and VIIRS data. Discussions are presented in Sections IV. Finally, Section V concludes this article.

II. Data and Methodology

A. SST Data From COCTS/HY-1D

The Chinese HY-1D satellite is the follow-up mission to the HY-1A and HY-1B satellites and was launched on June 11, 2020. It is a PM satellite with an overpass time of 13:30 $\pm$ 30 min local time at the ascending node; this satellite is equipped with five payloads, similar to the HY-1C satellite, including the COCTS, a coastal zone imager, an ultraviolet imager, a satellite calibration spectrometer, and a satellite-based automatic identification system receiver. The Chinese ocean color satellite constellation, which comprises two satellites, HY-1C and HY-1D, has been complete since the launch of the HY-1D satellite. The HY-1C satellite, which was launched on September 7, 2018, is an AM satellite with an overpass time of 10:30 $\pm$ 30 min local time at the descending node [11], [29]. The joint observations of HY-1C and HY-1D increase the observation time and improve the global coverage. The COCTS instruments on the two satellites can detect the global ocean and land four times every day and provide daily ocean color and daytime and nighttime SST data.

The COCTS is a moderate-resolution imaging scanner with a spatial resolution of 1.1 km at the nadir and a viewing swath width of 3000 km. The sensor measures signal in eight visible and near-infrared bands and two TIR bands. The spectral ranges of the two TIR bands are 10.30–11.30 μm (with a central wavelength at 10.8 μm) and 11.50–12.50 μm (with a central wavelength at 12.0 μm). The designed noise-equivalent changes in temperature are both 0.20 K under the measurement condition of 300 K, while the evaluated values ranged from 0.02 to 0.03 K during the on-orbit testing activity. The sensor can measure BTs within a range of 200–320 K.

The SSTs used in this study were derived from the bright temperatures of the two TIR bands of the COCTS (i.e., the Level-1B (L1B) standard product of the COCTS). These L1B data can be found at the Ocean Color Satellite Data Service Center,[1] operated by the National Satellite Ocean Application Service of the Ministry of Natural Resources in China.

The SST retrieval and clear-sky mask methods used by COCTS/HY-1D are the same as those of the HY-1C COCTS [11]. The SST retrieval algorithm is the modified version of the NLSST algorithm of Walton *et al.* [1]. The NLSST algorithm for the two TIR bands of the COCTS can be described as follows:

$$\mathrm{SST} = \mathrm{a}_0 + (\mathrm{a}_1 + \mathrm{a}_2 S_\theta) T_{11} + [\mathrm{a}_3 + \mathrm{a}_4 T_{\mathrm{sfc}} + \mathrm{a}_5 S_\theta](T_{11} - T_{12}) + \mathrm{a}_6 S_\theta \quad (1)$$

where $S_\theta = \sec\theta - 1$, θ is the sensor zenith angle, T_{11} and T_{12} are the BTs of the TIR bands of the COCTS at 10.8 and 12.0 μm, respectively, a_0 –a_6 are the algorithm coefficients, and T_{sfc} is the reference SST used as the first guess. In this study, T_{sfc} is derived from the COCTS by an MCSST. The equation form and coefficients of the MCSST algorithm are the same as those utilized for HY-1C; see [11, formula (1) and Table II]. The algorithm coefficients in formula (1) are improved by the regression method [11], [15], [16], [24], [25], [30]–[34] and detailed in Table I.

The coefficients listed in Table I differ between the daytime and the nighttime and were separately applied in the daytime and nighttime COCTS/HY-1D SST retrievals. The input data of T_{11} and T_{12} in formula (1) are in units of Kelvin, and the SSTs output by both the MCSST and NLSST algorithms are in units of degree Celsius (°C).

Because the satellite data were improved during the on-orbit testing activity of HY-1D before April 2021 (the improvement for the thermal channels is the striping removal), the SST data acquired in this study were collected in the time period from April 26 to August 31, 2021. Fig. 1 shows example HY-1D SST products covering Gulf Stream waters in the daytime and the nighttime.

From the SST maps displayed in Fig. 1, a warm ocean current (i.e., the Gulf Stream) can be seen flowing northeast along the coast of the USA to the area near approximately 68 °W, 38 °N and eastward from there. The white pixels in the figure are regions in which the water was covered by clouds.

B. VIIRS SSTs

The VIIRS is an instrument aboard the joint NASA/NOAA S-NPP satellite and the NOAA-20 satellite (the NOAA-20 satellite was previously known as the joint polar satellite system). The VIIRS has 22 spectral bands ranging from 412 nm to 12 μm. The SST data used in this study were derived from the VIIRS on the S-NPP satellite and collected from the two IR bands (the same as those of the COCTS) of the VIIRS and downloaded from NASA's Ocean Color Web, which is supported by the Ocean Biology Processing Group at NASA's Goddard Space Flight Center.[2] The accuracy of the VIIRS SST was declared on its website[3] and Minnett *et al.* [35]. The mean bias (Mean), SD, RMSE, median, and robust standard deviation (RSD) of the VIIRS SST at its highest quality level (i.e., the quality level flag is equal to 0) are –0.126, –0.129, 0.480, and 0.340 °C validated against subsurface buoy SST, respectively [35]. The VIIRS SST has high accuracy and can be used for cross-validation for the COCTS SST.

Fig. 2 shows examples of VIIRS SSTs covering the same Gulf Stream area as that shown in Fig. 1. The VIIRS instrument

[1][Online]. Available: https://osdds.nsoas.org.cn/

[2][Online]. Available: https://oceancolor.gsfc.nasa.gov/

[3][Online]. Available: https://oceancolor.gsfc.nasa.gov/atbd/sst/#sec_1

TABLE I
COEFFICIENTS OF SST RETRIEVAL ALGORITHMS OF COCTS/HY-1D

Algorithm	a_0	a_1	a_2	a_3	a_4	a_5	a_6
NLSST (Daytime)	-282.387880	1.044340	0.020962	0.484180	0.071798	0.747450	-4.997405
NLSST (Nighttime)	-281.987356	1.043650	0.025165	0.433639	0.074175	0.610433	-5.873327

TABLE II
STATISTICS BETWEEN SSTS FROM COCTS/HY-1D AND *IN SITU* MEASUREMENTS FROM IQUAM

	N	Mean bias (°C)	SD (°C)	RMSE (°C)	Median (°C)	RSD (°C)
Daytime	1158	-0.01	0.65	0.65	0.04	0.51
Nighttime	510	-0.10	0.71	0.71	-0.07	0.47

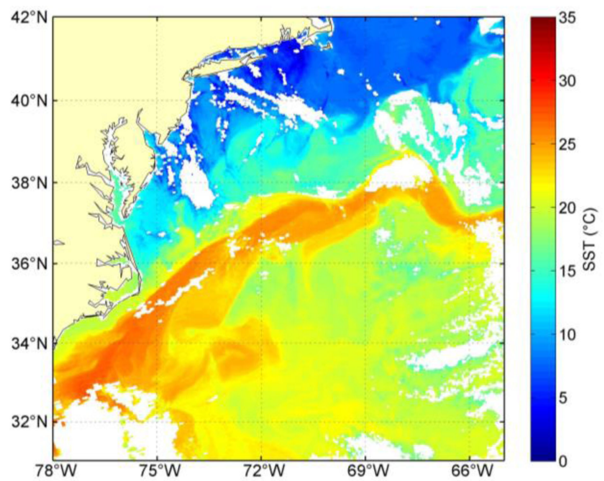

(a)

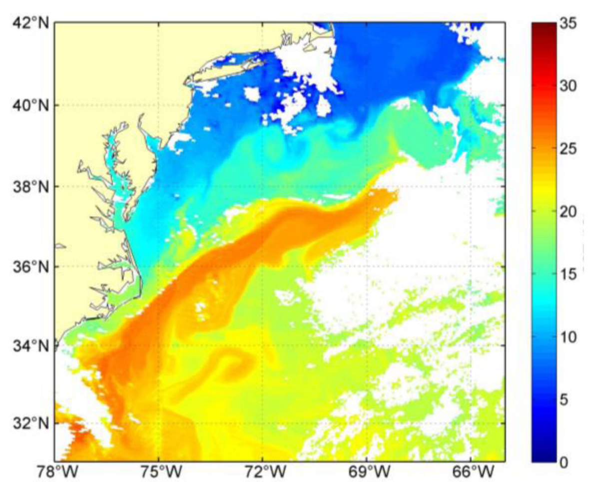

(b)

Fig. 1. SSTs derived from the COCTS on the HY-1D satellite covering Gulf Stream waters acquired at (a) 17:35 UTC and (b) 06:20 UTC on April 27, 2021. (a) Daytime SSTs. (b) Nighttime SSTs.

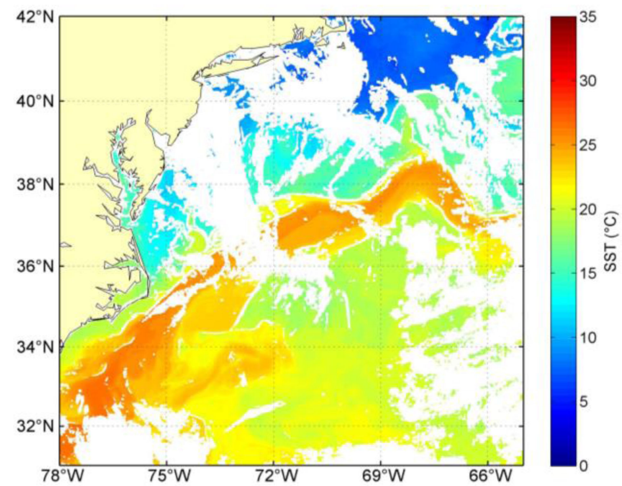

(a)

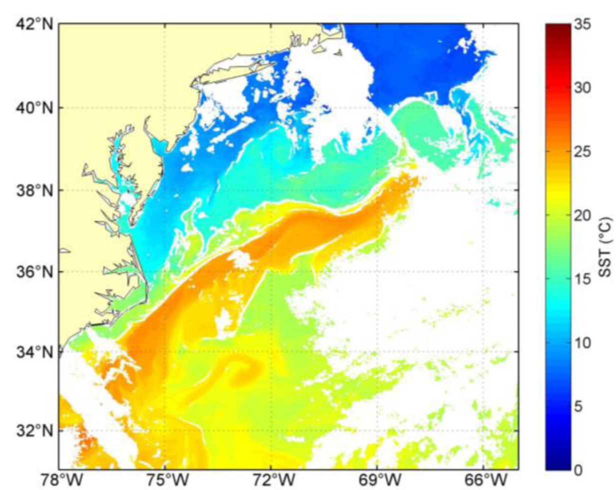

(b)

Fig. 2. Sea surface temperature from the VIIRS on the S-NPP satellite covering Gulf Stream waters acquired at (a) 18:12 UTC and (b) 06:48 UTC on April 27, 2021. (a) Daytime SSTs. (b) Nighttime SSTs.

aboard the S-NPP and the COCTS instrument aboard the HY-1D satellite monitor SSTs near-simultaneously with a delay of no more than 40 min.

The SSTs shown in Figs. 1 and 2 represent the Level-2 products of the COCTS and the VIIRS, respectively, i.e., they are single-scene data products. In the next section, we will cross-validate the SSTs shown in Fig. 1 against those shown in Fig. 2.

Because the HY-1D and S-NPP satellites have almost the same overpass times at their descending and ascending nodes, in this study, NASA's standard mapped (L3M) SST products were also used to evaluate the consistency of the SSTs derived from the COCTS and the VIIRS.

C. In Situ Data

The *in situ* SSTs used in this study were the bulk water temperatures collected by iQuam[4] developed by the Center for

[4][Online]. Available: www.star.nesdis.noaa.gov/sod/sst/iquam/

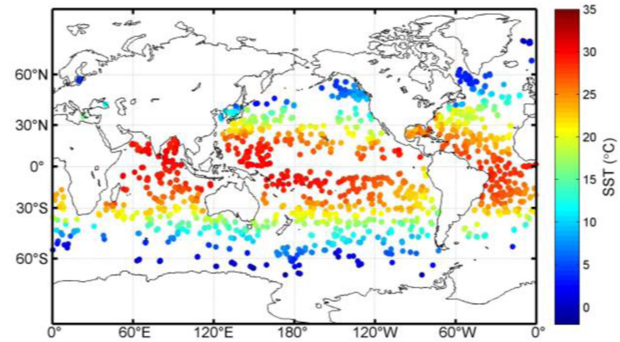

Fig. 3. Highest-quality water temperatures measured at depths above 1 m from iQuam in June 2021.

Satellite Applications and Research and the NOAA National Environmental Satellite, Data, and Information Service [35]. In iQuam v2.10, the version used in this study, the *in situ* SST data types include data recorded by Argo floats, conventional drifters, high-resolution drifters, tropical moorings, coastal moorings, coral reef water buoys, conventional ships, and integrated marine observing system ships. Only the highest quality iQuam datasets (i.e., datasets with level-5 quality flags) measured at water depths above 1 m were used for the evaluations conducted in this study. Fig. 3 shows the selected *in situ* water temperature data of iQuam in June 2021, as an example. The data collected in the period from April 26 to August 31, 2021 were used to validate the HY-1D SSTs. The total number of selected *in situ* water temperature datasets is 21 518 and 16 164 in the daytime and the nighttime, respectively. They range from –1.84 to 32.06 °C with a mean of 25.55 °C for daytime data and range from –1.83 to 31.87 °C with a mean of 24.91 °C for nighttime data.

D. Match-Up and Validation for Evaluation

To obtain a nearly simultaneously remotely sensed SST dataset from satellite and *in situ* measurements taken at the same location for the validation comparison, we chose matching datasets, for which the time interval between the *in situ* and satellite measurements was ≤ 4 h, and the distance between the *in situ* measurement locations and clear-sky pixels was ≤ 2.5 km. Moreover, the number of pixels in each remote sensing SST dataset selected for matching was greater than 10, i.e., the number of pixels capturing clear-sky conditions should represent no less than half of all pixels in the raw data. The standard deviation of the selected remote sensing SST data was less than 0.5 °C. The mean values of the remote sensing SST data and the *in situ* SSTs compose a pair of matching data. After this match-up processing, 1158 (daytime) and 510 (nighttime) data pairs were selected for the COCTS SST validation in this study; these numbers are displayed in Fig. 4 and detailed in Table II in the next section. It is noted that the data pairs during the daytime are much more than that at the nighttime. The reason is that the daytime *in situ* measurements selected are more than that at the nighttime.

To evaluate the SSTs derived from the COCTS by performing a cross-validation against VIIRS data, in this study, we selected

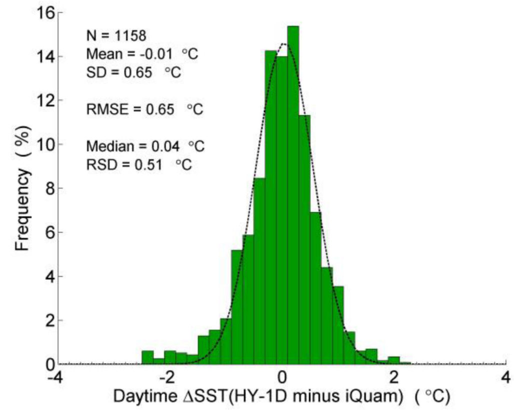

(a)

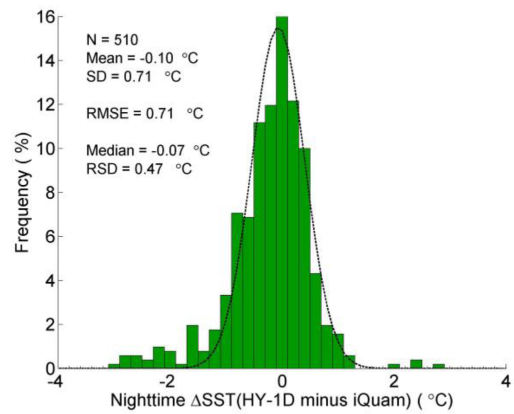

(b)

Fig. 4. Histograms of SST biases between the COCTS data and *in situ* measurements from iQuam in the (a) daytime and (b) nighttime during the period from April 26 to August 31, 2021. The dotted black lines in the figures represent the Gaussian-distributed probability density function line fit to the data with the median value applied as the mean and the RSD^2 value applied as the variance.

the mean SST data values in a 5 × 5-pixel box around the cross-validation points in Figs. 1 and 2 to compose a matched dataset. These cross-validation points composed a grid from 78 to 65 °W and from 31 to 42 °N with an interval of 0.5°.

To evaluate the consistency of the SST data derived from the COCTS and the VIIRS, we directly compared the L3M data acquired at the same time period to those from the COCTS and the VIIRS.

The mean bias (Mean), SD, RMSE, median, and RSD were used in this study to describe the differences between the SSTs derived from the COCTS and the *in situ* or VIIRS measurements. The statistics used herein were also applied in [11], [27], [28], [37], and [38]. The median and RSD used herein can be derived from biases data by fitting the data with a Gaussian-distributed probability density function [37].

III. Results

A. Validation Against In Situ Measurements

Histograms of the SST biases determined between the COCTS/HY-1D and *in situ* measurements from iQuam in both the daytime and the nighttime during the period from April 26 to August 31, 2021, are presented in Fig. 4. The validation statistics, including the number of matching datapoints (*N*), mean, SD, RMSE, median, and RSD, are also shown in the figure and listed in Table II. As shown in Fig. 4(a) and (b), the bias histograms have a quasi-Gaussian shape, and the median and the RSD were derived by fitting a Gaussian-distributed probability density function to the data; see the dotted black lines in the figures.

As listed in Table II, the SST RMSEs are 0.65 and 0.71 °C and the SST SDs are 0.65 and 0.71 °C in the daytime and the nighttime, respectively; the SST RSDs are 0.51 and 0.47 °C in the daytime and the nighttime, respectively. The RSDs are smaller than the corresponding SDs because the RMSEs and SDs represent validation results obtained for all satellite-derived SST data, and some SST measurements may be covered by light clouds or unscreened cloud contamination in the clear-sky/cloud-masking processing methods; see the data with biases less than 2 °C in Fig. 4(b). Furthermore, at night, only two TIR bands' BTs can be used to detect clouds [11]. The median and RSD values were derived from the SST data biases minus the *in situ* measurements by fitting. This means that the median and RSD values represent statistics with outliers removed. Assuming that the cloud-screening process is fairly efficient (i.e., the majority of data are indeed cloud free), robust statistics (i.e., the median and RSD values) more fairly characterize the performance of the retrieval method when it is applied to the kind of clear-sky data for which it is truly intended [37]. Therefore, the RSD can be used to characterize the performance of the COCTS/HY-1D sensor.

Fig. 5(a) and (b) shows scatterplots of the matching SST dataset derived from the COCTS/HY-D and *in situ* measurements collected during the daytime and the nighttime, respectively. The scatterplots are distributed uniformly and reveal SSTs ranging from –1.81 to 32.52 °C in the daytime and from –1.40 to 31.64 °C at night. The validation results presented in Fig. 4(a) and (b) and Table II are realistic, indicating SSTs within reasonable ranges.

As shown in Fig. 5, the HY-1D nighttime SST has a bit bigger difference in the range of 0–5 °C. The cause may be the cloud detection at night for the COCTS using only two TIR bands' BTs, while the signal of red band at the wavelength of 675 nm can be used only in the daytime [11]. As a result, some pixels covered by light clouds or unscreened cloud contamination at night were created as clear sky, and their retrieval SSTs were a bit lower than the *in situ* measurements, as shown in Fig. 5(b).

The locations of the SST pairs matched between the COCTS-derived SSTs and iQuam *in situ* measurements are shown in Fig. 6. The colors of the location points correspond to the SST bias value.

As shown in Fig. 6(a) and (b), the SST bias values (collected in both the daytime and the nighttime) validated against the *in situ* measurements from iQuam are dispersed throughout the global ocean with no outstanding geographic distribution characteristics. The SSTs derived from COCTS/HY-1D have consistent accuracy throughout the global ocean waters.

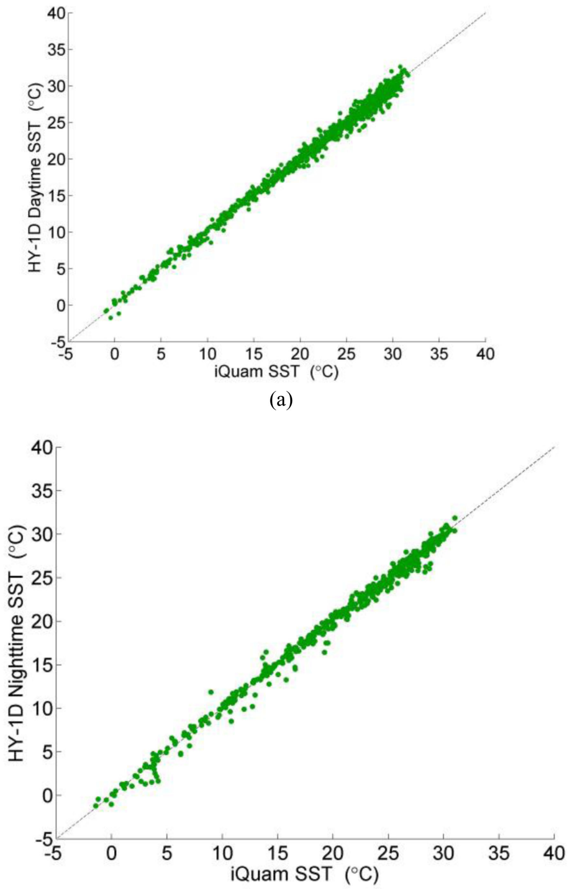

(a)

(b)

Fig. 5. Comparisons of the SST scatterplots derived from COCTS/HY-1D with *in situ* measurements derived from iQuam in the (a) daytime and (b) nighttime during the period from April 26, 2021 to August 31, 2021.

B. Cross-Validation Against VIIRS Data

Taking the SST data shown in Figs. 1 and 2 as a case study, we validate the SSTs derived from COCTS/HY-1D against those derived from VIIRS/S-NPP. The comparisons are shown with scatterplots in Fig. 7.

The number of matching datapoints used for the cross-validations (N) and the RMSE values is also presented in Fig. 7. The RMSEs are 0.53 °C in the daytime and 0.47 °C at night.

C. Comparison With VIIRS/S-NPP Observations

The global SST mapped products derived from the COCTS were temporally and spatially aggregated onto a georeferenced Earth grid over a defined period by a binning algorithm [39]. The mapped COCTS SSTs evaluated in this study were the daily, eight-day, and monthly products georeferenced onto a Plate Carrée projection with a grid size of 9.2 km. The grid size and period of these products are the same as those of NASA's standard L3M SST product. Therefore, these data can be directly compared with the VIIRS L3M products to evaluate their consistency.

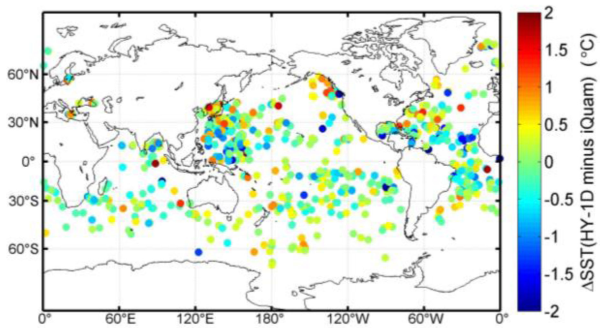

(a)

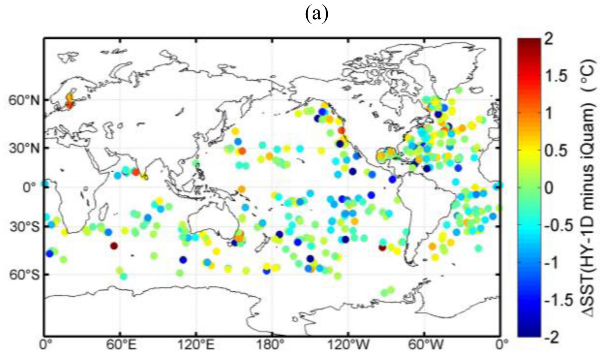

(b)

Fig. 6. Locations of the SST biases shown in Fig. 4 in the (a) daytime and (b) nighttime.

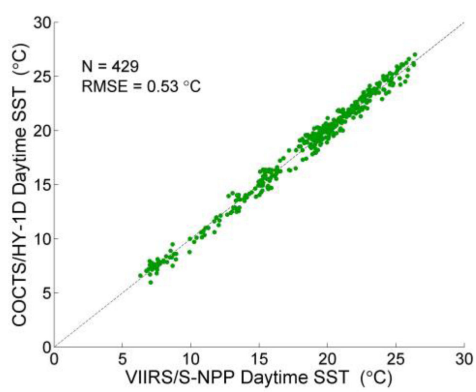

(a)

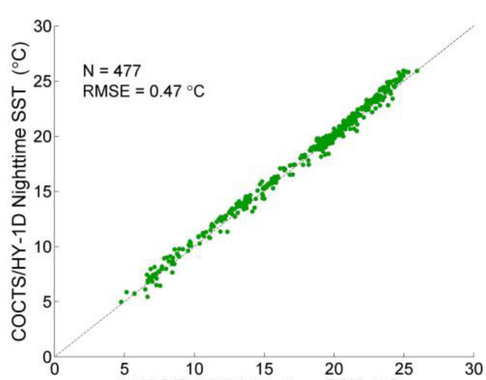

(b)

Fig. 7. Scatterplot comparisons of the SSTs derived from COCTS/HY-1D shown in Fig. 1 with those derived from VIIRS/S-NPP shown in Fig. 2 in the (a) daytime and (b) nighttime.

Figs. 8 and 9 present examples of the daily, eight-day, and monthly global gridded daytime and nighttime SST maps derived from the COCTS, respectively. The corresponding SST maps derived from VIIRS/S-NPP are also presented in Figs. 8 and 9 for comparison.

As shown by the SST maps in Figs. 8(a) and 9(a), COCTS/HY-1D can cover the whole global ocean twice a day regardless of the cloud or sea ice/snow coverage. The comparisons of the SSTs derived from the COCTS with those derived from the VIIRS in Figs. 8 and 9 show a lack of large SST differences between the two spaceborne sensors. We quantitatively evaluated the consistency of the daily gridded SSTs derived from COCTS/HY-1D with those derived from VIIRS/S-NPP. Figs. 10 and 11 show the comparison results of the SSTs shown in Fig. 8(a) with (b) and of those shown in Fig. 9(a) with (b).

As a case study, Fig. 10 shows the density scatterplots comparing the COCTS-derived SSTs with those derived from the VIIRS during both the daytime and the nighttime on June 18, 2021. Fig. 11 shows histograms of the SST biases shown in Fig. 10. The N, mean bias, SD, RMSE, median, and RSD statistics are also presented in Figs. 11(a) and (b).

Figs. 10 and 11 show that the SSTs derived from the COCTS and displayed in Figs. 8(a) and 9(a) are consistent with those derived from the VIIRS and shown in Figs. 8(b) and 9(b), with daytime and nighttime RMSEs of 0.60 and 0.73 °C, respectively, and daytime and nighttime RSDs of 0.47 and 0.52 °C, respectively. It is noted that there are more negative values of the differences between the COCTS and the VIIRS particularly for the nighttime shown in Fig. 11. The comparison results shown in Fig. 11 are the differences of the gridded SSTs between the COCTS and the VIIRS. The gridded SSTs are generated by the binning algorithm from the Level-2 SST products. The SST in a grid point is the average value of the Level-2 SST measurements under clear sky in its gridded water area. Its value would become lower if there was a part of pixels contaminated by unscreened cloud in its gridded bin. It is because that the retrieval SST would be lower if its pixel is covered by light cloud. As mentioned above, the cloud detection processing method for the COCTS is not effective enough for some conditions, such as light cloud covering, so that a few gridded SSTs of the COCTS become a bit lower. For the nighttime SST, its cloud detection was completed by only two TIR bands [11]. As a result, there were more unscreened cloud contamination pixels in nighttime SST products. The RMSEs are statistically analyzed from the comparison data, including the negative values of the difference between the COCTS and the VIIRS, which is the reason why the RSDs are also used for evaluation of the SST from the COCTS.

Fig. 12 shows time-series results obtained for the comparison between the daily gridded SSTs derived from COCTS/HY-1D and those derived from VIIRS/S-NPP from April 26 to August 31, 2021. The methods used to calculate the statistical values for each day are the same as those used to obtain the values shown in Fig. 11. Although small amplitude cycles exist in the figure, the mean bias, SD, median, RSD, and RMSE trend lines, shown in Fig. 12(a) and (b), indicate that both the daytime and nighttime SSTs derived from the COCTS remain stable over time. For the

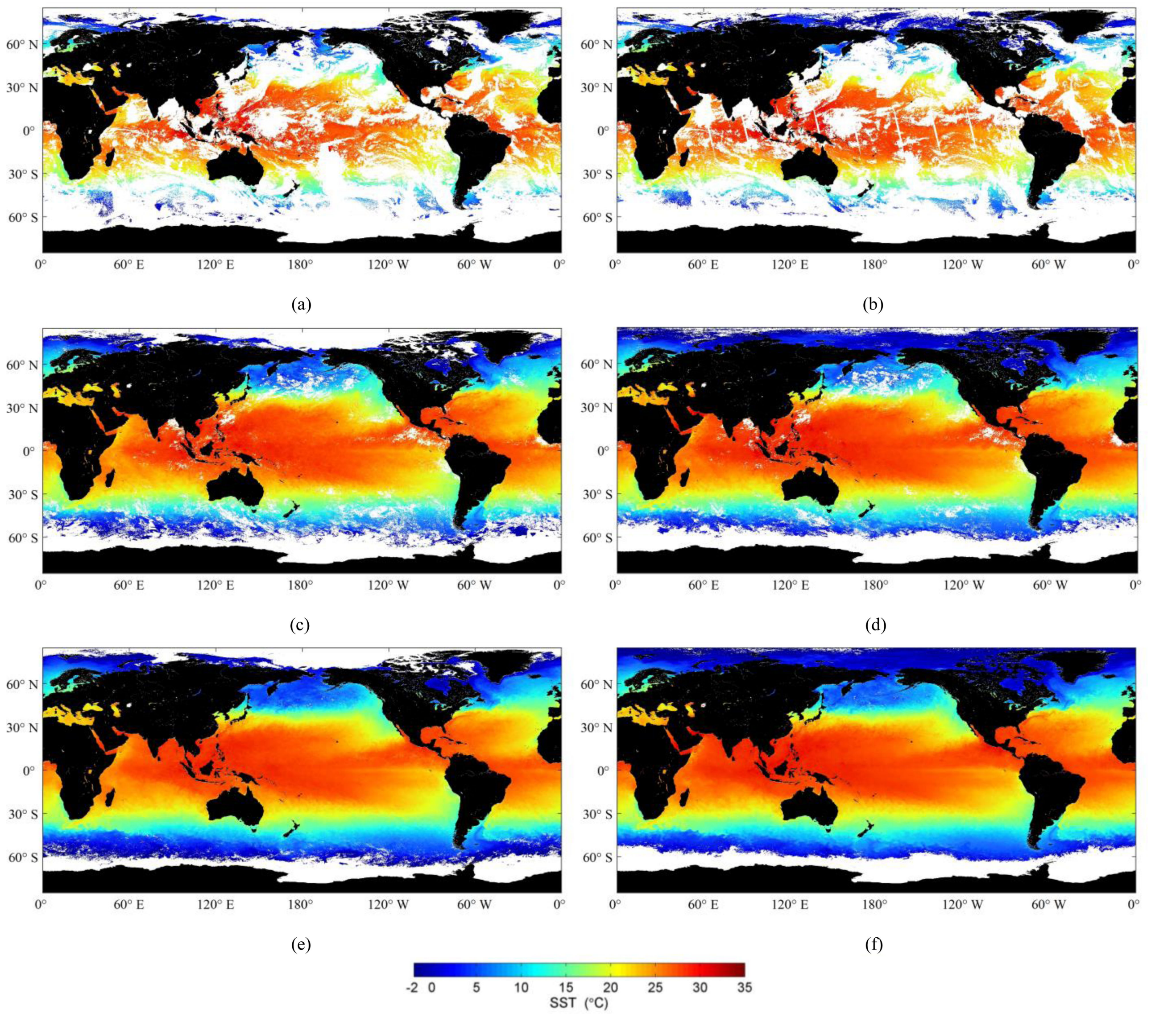

Fig. 8. Daytime SSTs derived from COCTS/HY-1D and VIIRS/S-NPP. (a) Daily SSTs (June 18, 2021), COCTS/HY-1D. (b) Daily SSTs (June 18, 2021), VIIRS/S-NPP. (c) Eight-day SSTs (June 18–25, 2021), COCTS/HY-1D. (d) Eight-day SSTs (June 18–25, 2021), VIIRS/S-NPP. (e) Monthly SSTs (June 2021), COCTS/HY-1D. (f) Monthly SSTs (June 2021), VIIRS/S-NPP.

small amplitude cycles in the figure, the reason can be explained as follows. The SSTs are measured at different solar zenith angles (local times) in such a wide swath Level-2 product of about 3000 km for the COCTS or the VIIRS. The orbit of HY-1D is not exactly the same as that of S-NPP. So, the differences of the measured local times also exist at the same geographical location between the two satellites' observation products, particularly for the data at the edges of the view fields. The SST changes at different local times due to the solar heating or heat radiation. It means that the COCTS and the VIIRS measure the SST of the same water area at different local times. The intraday variation of the SST and the repeated orbital cycles of the two satellites is the cause of the cycles of the statistics shown in Fig. 12.

The statistical values (means ± SDs), including the daily mean biases, SDs, medians, RSDs, and RMSEs, shown in Fig. 12, are detailed in Table III.

TABLE III
STATISTICS (MEAN ± SDs) OF THE SSTs DERIVED FROM COCTS/HY-1D AND VIIRS/S-NPP FROM APRIL 26 TO AUGUST 31, 2021

	Mean bias (°C)	SD (°C)	Median (°C)	RSD (°C)	RMSE (°C)
Daytime	-0.05±0.05	0.67±0.06	-0.03±0.05	0.49±0.04	0.67±0.06
Nighttime	0.03±0.05	0.81±0.06	0.07±0.06	0.58±0.05	0.81±0.06

As shown in Fig. 12 and listed in Table III, the daily mean biases obtained through the SST comparison during the period from April 26 to August 31, 2021, are –0.05 ± 0.05 °C for daytime SSTs and 0.03 ± 0.05 °C for nighttime SSTs. The daily mean RSDs are 0.49 ± 0.04 °C for daytime SSTs and 0.58 ± 0.05 °C for nighttime SSTs. The daily mean RMSEs are 0.67 ± 0.06 °C for daytime SSTs and 0.81 ± 0.06 °C for nighttime SSTs. The results indicate that both the daytime and nighttime

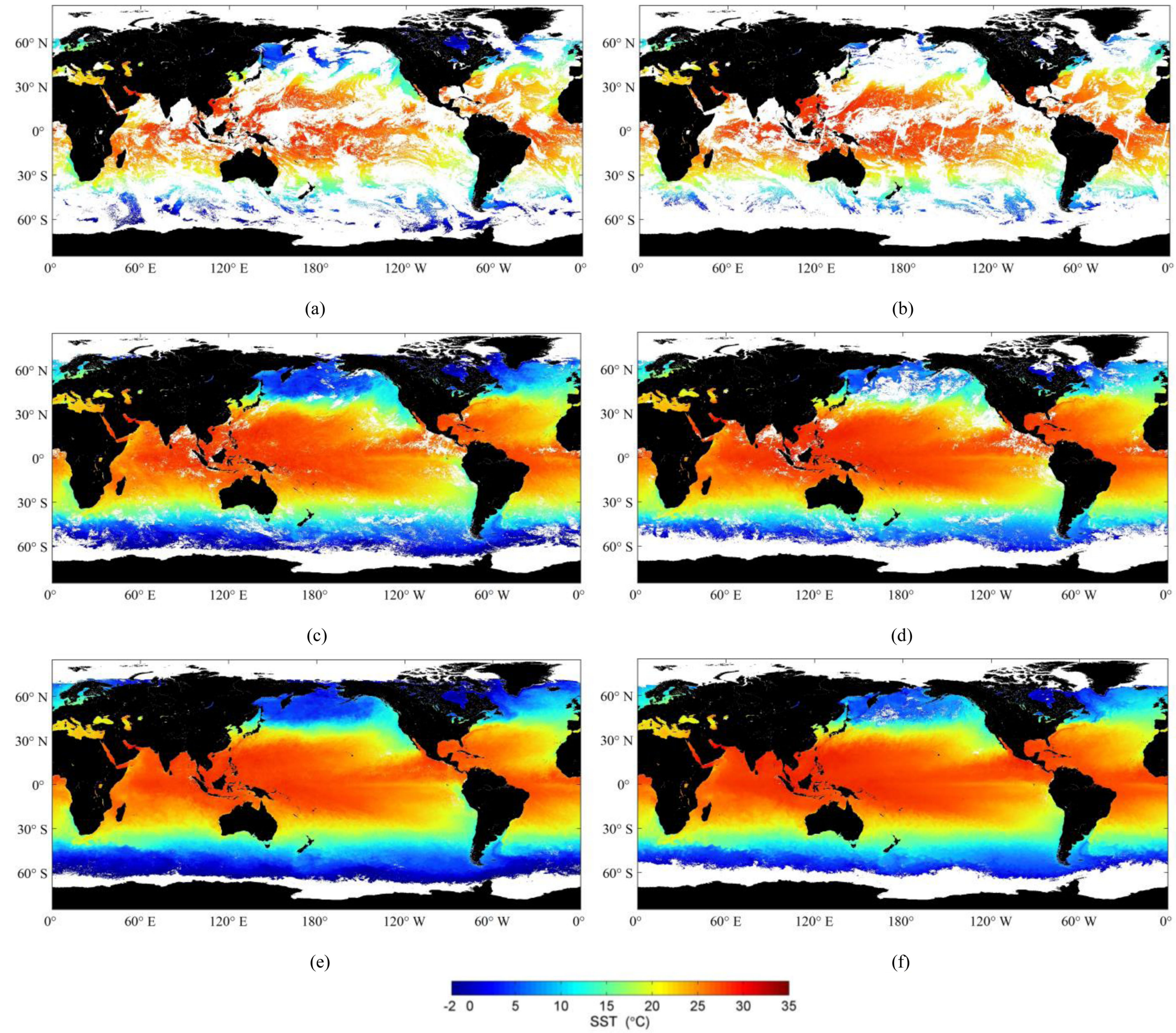

Fig. 9. Nighttime SSTs derived from COCTS/HY-1D and VIIRS/S-NPP. (a) Daily SSTs (June 18, 2021), COCTS/HY-1D. (b) Daily SSTs (June 18, 2021), VIIRS/S-NPP. (c) Eight-day SSTs (June 18–25, 2021), COCTS/HY-1D. (d) Eight-day SSTs (June 18–25, 2021), VIIRS/S-NPP. (e) Monthly SSTs (June 2021), COCTS/HY-1D. (f) Monthly SSTs (June 2021), VIIRS/S-NPP.

SSTs derived from the COCTS are consistent with those derived from VIIRS/S-NPP.

IV. Discussion

Notably, the numerical differences shown in Fig. 4(a) and (b) contain more negative values than positive values; this can be seen in the histograms on the left-hand side of Fig. 4(a) and (b), i.e., in the differences smaller than –2 °C or greater than 2 °C. The reason for this result is that it is difficult to discern pixels covered by light clouds in the clear-sky/cloud-masking processing without remote sensing measurements obtained at short-wave IR bands [11], [29]. A more effective cloud detection method for the COCTS needs to be developed in the further.

Conventional statistics (e.g., mean ± SD or RMSE) are considered to be informative of the performance of the entire SST processing system, including the effects of imperfect cloud screening and the sensitivity of the retrieval method to residual unscreened cloud contamination; the median and RSD values, in contrast, are derived from the data by fitting a Gaussian-distributed probability density function [11], [37]. In this study, assuming that the cloud-screening process is fairly efficient (i.e., that the majority of data are indeed cloud-free), the robust statistics (i.e., the median and RSD) characterize the performance of the COCTS, and its retrieval method more fairly than the conventional statistics when the method applied to clear-sky data, as it is truly intended to be used with these data [37]. Therefore, the RSDs [e.g., 0.51 and 0.47 °C against the *in situ* iQuam data, as shown in Fig. 4(a) and (b)] characterize the

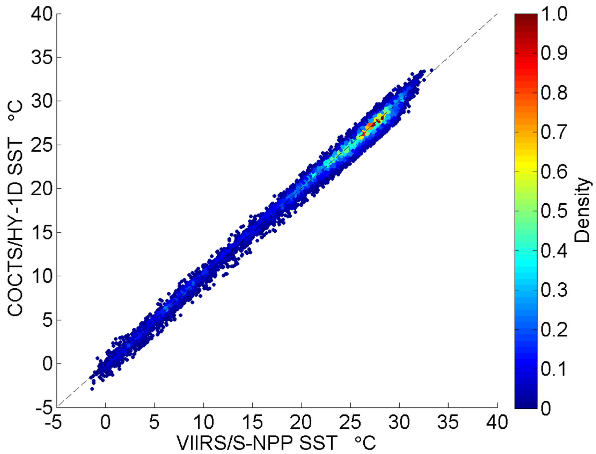

(a)

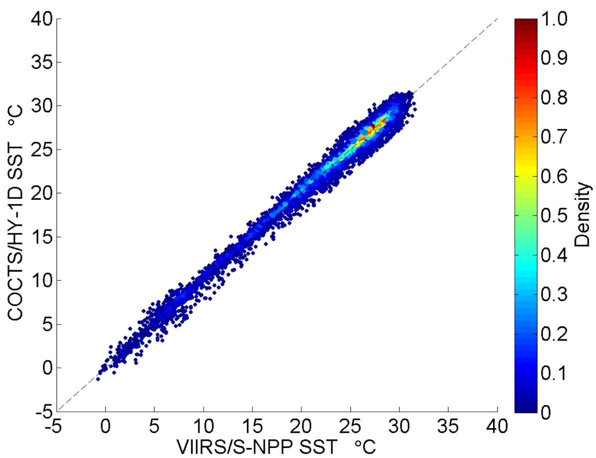

(b)

Fig. 10. Comparisons of the density scatterplots of the daily global SSTs derived from COCTS/HY-1D and VIIRS/S-NPP and acquired during the (a) daytime and (b) nighttime on June 18, 2021.

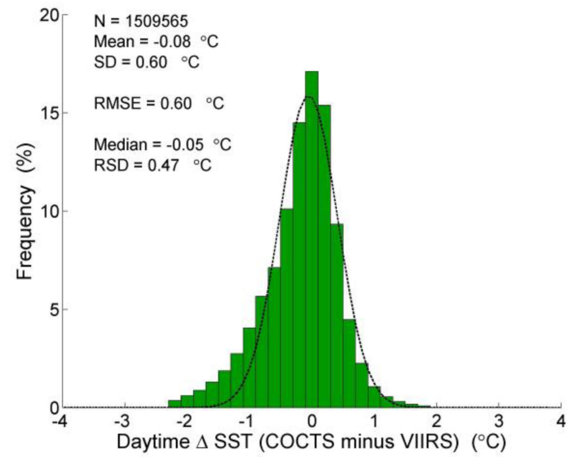

(a)

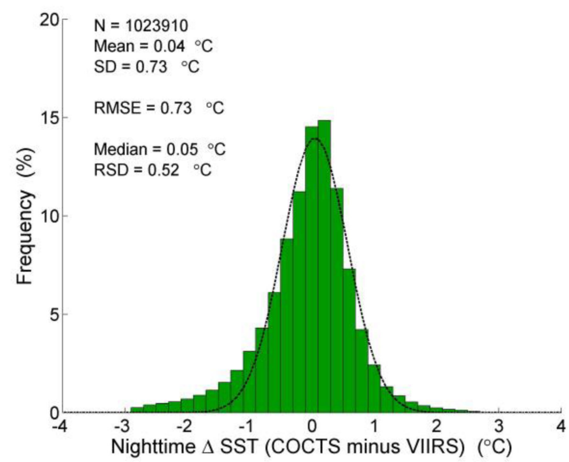

(b)

Fig. 11. Histograms of the SST differences between COCTS/HY-1D and VIIRS/S-NPP during the (a) daytime and (b) nighttime on June 18, 2021. The dotted black lines in the figures represent the Gaussian-distributed probability density function fitted line with the median applied as the mean and the RSD^2 value applied as the variance.

performance of the SSTs derived from clear-sky measurements collected by COCTS/HY-1D used in this study.

Statistical analysis results differ when different match-up methods or spatiotemporal windows are used. For example, the RMSEs are 0.65 and 0.71 °C for the daytime and nighttime SSTs from COCTS/HY-1D with a spatiotemporal matching window of 4 h and 2.5 km; if the spatiotemporal matching window is converted into 2 h and 2.5 km, these values become 0.65 and 0.68 °C; with a spatiotemporal matching window of 1 h and 2.5 km, these values become 0.60 and 0.66 °C; and with a spatiotemporal matching window of 0.5 h and 2.5 km, these values become and 0.52 and 0.62 °C, respectively. Table IV lists evaluation statistics, including the number of matching datapoints, mean bias, SD, median, RSD, and RMSE values, obtained by comparing the COCTS/HY-1D-derived SSTs against *in situ* measurements of iQuam with different temporal match-up windows.

As detailed in Table IV, the SD, RSD, and RMSE values decrease as the temporal match-up window decreases, and the number of matching datapoints (i.e., the *N* value in Table IV) and the confidence of the evaluation statistics simultaneously decrease. Therefore, the SST evaluation results are obtained under specific validation conditions, including specific spatiotemporal matching windows and other match-up processing methods.

TABLE IV
STATISTICS BETWEEN SSTS DERIVED FROM COCTS/HY-1D AND *IN SITU* MEASUREMENTS FROM IQUAM WITH DIFFERENT TEMPORAL MATCH-UP WINDOWS

	Temporal matching window (hrs)	N	Mean bias (°C)	SD (°C)	Median (°C)	RSD (°C)	RMSE (°C)
Daytime	4	1158	-0.01	0.65	0.04	0.51	0.65
	2	587	-0.05	0.65	0.04	0.50	0.65
	1	279	-0.08	0.59	0.03	0.48	0.60
	0.5	121	0.00	0.52	0.11	0.44	0.52
Nighttime	4	509	-0.10	0.71	-0.07	0.47	0.71
	2	263	-0.07	0.68	-0.06	0.44	0.68
	1	129	-0.03	0.66	-0.03	0.46	0.66
	0.5	66	-0.11	0.64	-0.06	0.40	0.64

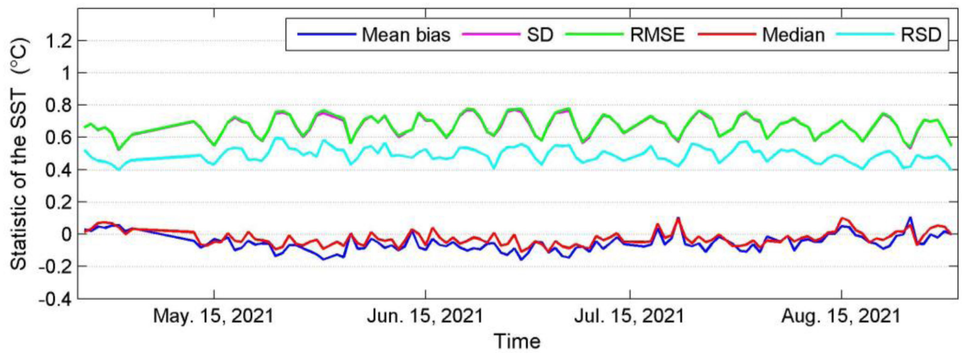

(a)

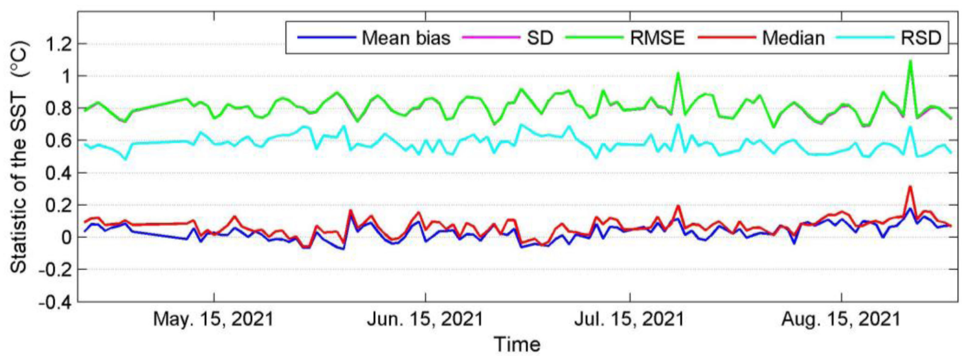

(b)

Fig. 12. Comparisons between the global daily gridded SSTs derived from COCTS/HY-1D and VIIRS/S-NPP from April 26, 2021 to August 31, 2021 in the (a) daytime and (b) nighttime.

V. Conclusion

As a new source of the satellite-based SST provided from the remote sensing instrument, the COCTS, aboard the HY-1D satellite, can detect global SSTs twice a day (once during the daytime and once at night).

In this study, the SSTs derived from COCTS/HY-1D were evaluated against *in situ* measurements collected from iQuam and remote sensing products derived from the VIIRS instrument on the S-NPP during the period from April 26 to August 31, 2021. RMSEs of 0.65 °C in the daytime and 0.71 °C at night were obtained by comparing the COCTS-derived SSTs to *in situ* measurements from iQuam. The cross-validation and consistency evaluation results showed that the SSTs derived from COCTS/HY-1D were consistent with those derived from VIIRS/S-NPP. All the evaluations conducted in this study indicated that the COCTS instrument aboard the HY-1D satellite observes SSTs with a satisfactory performance.

Evaluations were conducted in this study under specific match-up and quality control conditions in the global ocean. Different SST evaluation results may arise if different validation methods, temporal periods, or spatial data coverages are applied. More detailed analyses and evaluations will be considered in future investigations.

Acknowledgment

The authors would like to thank the NASA Goddard Space Flight Center, Ocean Ecology Laboratory, and Ocean Biology Processing Group for providing access to the VIIRS/S-NPP data, as well as the Center for Satellite Applications and Research and the National Oceanic and Atmospheric Administration National Environmental Satellite, Data, and Information Service for providing access to the *in situ* iQuam data.

References

[1] C. C. Walton, W. G. Pichel, J. F. Sapper, and D. A. May, "The development and operational application of nonlinear algorithms for the measurement of sea surface temperatures with the NOAA polar-orbiting environmental satellites," *J. Geophys. Res.*, vol. 103, no. C12, pp. 27999–28012, Nov. 1998, doi: 10.1029/98JC02370.

[2] F. J. Wentz, C. Gentemann, D. Smith, and D. Chelton, "Satellite measurements of sea surface temperature through clouds," *Science*, vol. 288, pp. 847–850, May 2000, doi: 10.1126/science.288.5467.847.

[3] R. W. Reynolds, N. A. Rayner, T. M. Smith, D. C. Stokes, and W. Wang, "An improved in situ and satellite SST analysis for climate," *J. Climate*, vol. 15, pp. 1609–1625, Jul. 2002. [Online]. Available: https://doi.org/10.1175/1520-0442(2002)015<1609:AIISAS>2.0.CO;2.

[4] C. Donlon *et al.*, "The global ocean data assimilation experiment high-resolution sea surface temperature pilot project," *Bull. Amer. Meteorol. Soc.*, vol. 88, no. 8, pp. 1197–1213, Aug. 2007, doi: 10.1175/bams-88-8-1197.

[5] M. Manzano-Sarabia, C. A. Salinas-Zavala, M. Kahru, S. E. Lluch-Cota, and A. Gonzaález-Becerril, "The impact of the 1997–1999 warm-SST and low-productivity episode on fisheries in the southwestern Gulf of Mexico," *Hydrobiologia*, vol. 610, no. 1, pp. 257–267, 2008, doi: 10.10007/s10750-008-9440-y.

[6] C. Paulino, M. Segura, and G. Chacón, "Spatial variability of jumbo flying squid (Dosidicus gigas) fishery related to remotely sensed SST and chlorophyll-a concentration (2004-2012)," *Fisheries Res.*, vol. 173, pp. 122–127, 2016, doi: 10.1016/j.fishres.2015.10.006.

[7] V. Banzon, T. M. Smith, T. M. Chin, C. Liu, and W. Hankins, "A long-term record of blended satellite and in situ sea-surface temperature for climate monitoring, modeling and environmental studies," *Earth Syst. Sci. Data*, vol. 8, pp. 165–176, 2016, doi: 10.5164/essd-8-165-2016.

[8] P. Chan and B. Gao, “A comparison of MODIS, NCEP, and TMI sea surface temperature datasets,” *IEEE Geosci. Remote Sens. Lett.*, vol. 2, no. 3, pp. 270–274, Jul. 2005, doi: 10.1109/LGRS.2005.846838.

[9] E. P. Mcclain, W. G. Pichel, C. C. Walton, Z. Ahmad, and J. Sutton, “Multi-channel improvements to satellite-derived global sea surface temperatures,” *Adv. Space Res.*, vol. 2, no. 6, pp. 43–47, 1982, doi: 10.1016/0273-1177(82)90120-X.

[10] E. P. Mcclain, W. G. Pichel, and C. C. Walton, “Comparative performance of AVHRR-based multichannel sea surface temperatures,” *J. Geophys. Res.*, vol. 90, no. C6, pp. 11587–11601, Nov. 1985, doi: 10.1029/JC090iC06p11587.

[11] X. Ye, J. Liu, M. Lin, J. Ding, B. Zou, and Q. Song, “Sea surface temperatures derived from COCTS onboard the HY-1C satellite,” *IEEE J. Sel. Topics Appl. Earth Observ. Remote Sens.*, vol. 14, pp. 1038–1047, 2021, doi: 10.1109/JSTARS.2020.3033317.

[12] P. L. Le Borgne, H. Roquet, and C. J. Merchant, “Estimation of sea surface temperature from the spinning enhanced visible and infrared imager, improved using numerical weather prediction,” *Remote Sens. Environ.*, vol. 115, pp. 55–65, 2011, doi: 10.1016/j.rse.2010.08.004.

[13] B. Petrenko, A. Ignatov, N. Shabanov, and Y. Kihai, “Development and evaluation of SST algorithms for GOES-R ABI using MSG SEVIRI as a proxy,” *Remote Sens. Environ.*, vol. 115, pp. 3647–3658, 2011, doi: 10.1016/j.rse.2011.09.003.

[14] B. Ai, Z. Wen, Y. Jiang, S. Gao, and G. Lv, “Sea surface temperature inversion model for infrared remote sensing images based on deep neural network,” *Infrared Phys. Technol.*, vol. 99, pp. 231–239, 2019, doi: 10.1016/j.infrared.2019.04.022.

[15] B. Petrenko, A. Ignatov, Y. Kihai, J. Stroup, and P. Dash, “Evaluation and selection of SST regressing algorithms for JPSS VIIRS,” *J. Geophys. Res. Atmos.*, vol. 119, pp. 4580–4599, 2014, doi: 10.1002/2013JD020637.

[16] K. A. Kilpatrick *et al.*, “A decade of sea surface temperature from MODIS,” *Remote Sens. Environ.*, vol. 165, pp. 27–41, 2015, doi: 10.1016/j.rse.2015.04.023.

[17] K. Hosoda and H. Qin, “Algorithm for estimating sea surface temperatures based on Aqua/MODIS global ocean data. 1 Development and validation of the algorithm,” *J. Oceanogr.*, vol. 67, pp. 135–145, 2011, doi: 10.1007/s10872-011-0007-6.

[18] K. Hosoda, H. Murakami, F. Sakaida, and H. Kawamura, “Algorithm and validation of sea surface temperature observation using MODIS sensors aboard Terra and Aqua in the Western North Pacific,” *J. Oceanogr.*, vol. 63, pp. 267–280, 2007, doi: 10.1007/s10872-007-0027-4.

[19] R. F. Vincent, R. F. Marsden, P. J. Minnett, K. A. M. Creber, and J. R. Buckley, “Arctic waters and marginal ice zones: A composite Arctic sea surface temperature algorithm using satellite thermal data,” *J. Geophys. Res.*, vol. 113, 2008, Art. no. C04021, doi: 10.1029/2007JC004353.

[20] R. M. Vavalli, “Retrieval of sea surface temperature from MODIS data in coastal water,” *Sustainability*, vol. 9, Nov. 2017, Art. no. 2032, doi: 10.3390/su9112032.

[21] P. K. Koner, “Daytime sea surface temperature retrieval incorporating mid-wave imager measurements: Algorithm development and validation,” *IEEE Trans. Geosci. Remote Sens.*, vol. 59, no. 4, pp. 2833–2844, Apr. 2021, doi: 10.1109/TGRS.2020.3008656.

[22] C. L. Gentemann, “Three way validation of MODIS and AMSR-E sea surface temperatures,” *J. Geophys. Res., Oceans*, vol. 119, pp. 2583–2598, 2014.

[23] M. A. Lee *et al.*, “Validation of JAXA/MODIS sea surface temperature in water around Taiwan using the Terra and Aqua satellites,” *Terr. Atmos. Ocean Sci.*, vol. 21, pp. 727–736, 2010.

[24] E. J. Kim *et al.*, “Satellite-derived SST validation based on in-situ data during summer in the East China Sea and Western North Pacific,” *J. Ocean Sci.*, vol. 45, no. 3, pp. 159–170, 2010.

[25] H. L. Qin, G. X. Chen, W. Q. Wang, D. X. Wang, and L. L. Zeng, “Validation and application of MODIS-derived SST in the South China Sea,” *Int. J. Remote Sens.*, vol. 35, pp. 4315–4328, 2014.

[26] Y. Hao, T. Cui, V. P. Singh, J. Zhang, R. Yu, and Z. Zhang, “Validation of MODIS sea surface temperature product in the coastal waters of the Yellow Sea,” *IEEE J. Sel. Topics Appl. Earth Observ. Remote Sens.*, vol. 10, no. 5, pp. 1667–1680, May 2017, doi: 10.1109/JSTARS.2017.2651951.

[27] H. Wang, L. Guan, and G. Chen, “Evaluation of sea surface temperature from FY-3C VIRR data in the Arctic,” *IEEE Geosci. Remote Sens. Lett.*, vol. 13, no. 2, pp. 292–296, Feb. 2016, doi: 10.1109/LGRS.2015.2511184.

[28] M. Yang, L. Guan, H. Beggs, N. Morgan, Y. K. Urihara, and M. Kachi, “Comparison of Himawari-8 AHI SST with shipboard skin SST measurements in the Australian region,” *Remote Sens.*, vol. 12, Apr. 2020, Art. no. 1237, doi: 10.390/rs12081237.

[29] X. Ye, J. Liu, M. Lin, J. Ding, B. Zou, and Q. Song, “Global ocean chlorophyll-a concentrations derived from COCTS onboard the HY-1C satellite and their preliminary evaluation,” *IEEE Trans. Geosci. Remote Sens.*, vol. 59, no. 12, pp. 9914–9926, Dec. 2021, doi: 10.1109/TGRS.2020.3036963.

[30] K. A. Kilpatrick, G. P. Podestá, and R. Evans, “Overview of the NOAA/NASA advanced very high resolution radiometer Pathfinder algorithm for sea surface temperature and associated matchup database,” *J. Geophys. Res.*, vol. 106, no. C5, pp. 9179–9197, May 2001, doi: 10.1029/1999JC000065.

[31] C. J. Donlon *et al.*, “Toward improved validation of satellite sea surface skin temperature measurements for climate research,” *J. Climate*, vol. 15, pp. 353–369, Feb. 2002. [Online]. Available: https://doi.org/10.1175/1520-0442(2002)015<0353:TIVOSS>2.0.CO;2

[32] P. J. Minnett, “Radiometric measurements of the sea-surface skin temperature: The competing roles of the diurnal thermocline and the cool skin,” *Int. J. Remote Sens.*, vol. 24, no. 24, pp. 5033–5047, 2003, doi: 10.1080/0143116031000095880.

[33] O. B. Brown and P. J. Minnett, “MODIS infrared sea surface temperature algorithm algorithm theoretical basis document version 2.0,” Univ. Miami, Coral Gables, FL, USA, Apr. 1999, pp. 1–83.

[34] B. Petrenko and J. Stroup, “Advanced clear-sky processor for oceans (ACSPO)-VIIRS, algorithm theoretical basis document, version 1.0,” SST Integrated Product Team, NPOESS Data Exploitation Project, and Office of Satellite and Product Operations, Suitland, MD, USA, Aug. 2013, pp. 1–60.

[35] P. J. Minnett *et al.*, “Skin sea-surface temperature from VIIRS on Suomi-NPP—NASA continuity retrievals,” *Remote Sens.*, vol. 10, Oct. 2020, Art. no. 3369, doi: 10.3390/rs12203369.

[36] F. Xu and A. Ignatov, “In-situ SST Quality Monitor (iQuam),” *J. Atmos. Ocean. Technol.*, vol. 31, pp. 164–180, Jan. 2014, doi: 10.1175/jtech-d-13-00121.1.

[37] C. J. Marchant and A. R. Harris, “Toward the elimination of bias in satellite retrievals of sea surface temperature 2 Comparison with in-situ measurements,” *J. Geophys. Res.*, vol. 104, no. C10, pp. 23579–23590, Oct. 1999, doi: 10.1029/1999JC900106.

[38] C. J. Merchant, P. L. Borgne, A. Marsouin, and H. Roquet, “Optimal estimation of sea surface temperature from split-window observations,” *Remote Sens. Environ.*, vol. 112, pp. 2469–2484, 2008, doi: 10.1016/j.rse.2007.11.011.

[39] J. W. Campbell, J. M. Blaisdell, and M. Darzi, “Level-3 SeaWiFS data products: Spatial and temporal binning algorithms,” NASA Goddard Space Flight Center, Greenbelt, MD, USA, NASA Tech. Memo. 104566, 1995, vol. 32.

Xiaomin Ye received the B.S. degree in optical information science and technology from Nankai University, Tianjin, China, in 2006, the master’s degree in physical oceanography from the First Institute of Oceanography, State Oceanic Administration, Qingdao, China, in 2009, and the Ph.D. degree in oceanic detection technology from the Ocean University of China, Qingdao, in 2017.

He is currently a Designer in charge of data processing for the Chinese HY-1C/D satellite with the National Satellite Ocean Application Service, Beijing, China. His research interests include electromagnetic wave scattering from the ocean surface and the application of ocean satellite data.

Jianqiang Liu received the B.S. degree in geophysics from Peking University, Beijing, China, in 1986, and the master’s degree in marine meteorology from the National Marine Environmental Forecasting Center, State Oceanic Administration, Beijing, in 1989.

He is currently with the National Satellite Ocean Application Service, Beijing. He is the Chief Designer of the ground application system with the Chinese–France Ocean satellite and new generational ocean color satellites. He was a Deputy Chief Designer of the ground application system for the HY-1 and HY-2 satellites. He is one of the founders of satellite ocean remote sensing in China and plays an important role in the development of Chinese ocean satellites and manned space flight. His research interests include ocean color and sea wave satellite data processing, applications of ocean remote sensing data, and Antarctic research.

Mingsen Lin (Member, IEEE) received the B.S. degree in applied mechanics from the National University of Defense Technology, Changsha, China, in 1984, and the Ph.D. degree in computational mathematics from the Computing Center, Chinese Academy of Sciences, Beijing, China, in 1992.

He is currently the Chief Designer of the ground application system for Chinese salinity satellites, synthetic aperture radar satellites, and new generational ocean dynamic satellites. He was also a Deputy Chief Designer of the ground application system for the HY-1 and HY-2 satellites, where he organized the framework for the Chinese ocean satellite outline and managed the construction of the ground application system for the Chinese ocean satellite with the National Satellite Ocean Application Service, Beijing. He is one of the Founders of satellite ocean remote sensing in China. He plays an important role in the development of Chinese ocean satellites and manned space flight. His research interests include ocean satellite data processing, remote sensing of the ocean, and associated applications.

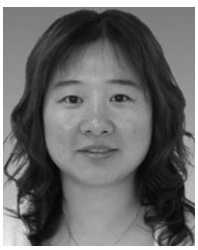

Jing Ding received the Ph.D. degree in physical oceanography from the Ocean University of China, Shandong, China, in 2004.

She has always focused on ocean color remote sensing and satellite data processing. Since 2004, she has been with the National Satellite Ocean Application Service, Beijing, China, where she is a Research Scientist in areas of satellite remote sensing, especially in satellite projects for ocean color and coastal environment monitoring. She is also the Head of the HY-1C/D Satellite Data Processing Group involved in the strategy and framework for satellite data processing as well as the algorithms related to ocean color products and applications.

Bin Zou received the B.S. degree in meteorology from Peking University, Beijing, China, in 1992, and the master's degree in marine meteorology from the National Marine Environmental Forecasting Center, State Oceanic Administration, Beijing, in 1995.

He is currently with the National Satellite Ocean Application Service, Beijing. He is a Deputy Chief Designer of the ground application system for HY-1C/D satellites. He went to Antarctica in 1995 to conduct Antarctic sea ice monitoring, research, and applications and to the Arctic in 1999 for Arctic Sea ice and sea fog research. He is involved in ocean remote sensing, satellite ground data processing system construction technology, ocean color satellite product processing algorithm and software, ocean oil spill monitoring, and remote sensing fishery applications.

Qingjun Song received the B.S. degree in applied physics from the Hefei University of Technology, Hefei, China, in 2001, and the M.S. degree in ocean technology from Dalian Ocean University, Dalian, China, in 2012.

He is currently a Researcher with the National Satellite Ocean Application Service, Ministry of Natural Resources, Beijing, China, and works on instrument calibrations and ocean remote sensing product validations with the HY-1 and HY-2 series satellites. His research interests include remote sensing and the absolute radiometric calibration of optical instruments.

Yue Teng received the B.S. degree in remote sensing from Shandong Agricultural University, Taian, China, in 2019. She is currently working toward the master's degree with the National Satellite Ocean Application Service, Beijing, China.

Her research interests include ocean remote sensing and satellite data processing.